

Article

Thermal-Mechanical Fatigue Behavior and Life Assessment of Single Crystal Nickel-Based Superalloy

Juan Cao ¹, Fulei Jing ² and Junjie Yang ^{3,*} ¹ Aero Engine Corporation of China, Beijing 100097, China² Aero Engine Academy of China, Aero Engine Corporation of China, Beijing 101304, China; jingfulei@163.com³ Institute for Aero Engine, Tsinghua University, Beijing 100084, China

* Correspondence: yangjunjie@tsinghua.edu.cn

Abstract: Thermal-mechanical fatigue (TMF) tests and isothermal fatigue (IF) tests were conducted using thin-walled tubular specimens under strain-controlled conditions. The results of TMF tests showed a strong correlation between mechanical behavior and temperature cycling. Under different phases of temperature and mechanical loading, the hysteresis loop and mean stress of the single crystal superalloy showed noticeable variations between the stress-controlled and strain-controlled conditions. In the strain-controlled TMF test, temperature cycling led to stress asymmetry and additional damage, resulting in a significantly lower TMF life compared to IF life at the maximum temperature. Moreover, the OP TMF life is generally lower than that of the IP TMF at the same strain amplitude. The Walker viscoplastic constitutive model based on slip systems was used to analyze the TMF mechanical behavior of the single crystal superalloy, and the change trends of the maximum Schmid stress, the maximum slip shear strain rate, and the slip shear strain range were analyzed, and their relationship with the TMF life was investigated. Finally, a TMF life prediction model independent of the loading mode and phase was constructed based on meso-mechanical damage parameters. The predicted TMF lives for different load control modes and phases fell within the twofold dispersion band.

Keywords: single crystal superalloy; thermal-mechanical fatigue; strain-controlled; cyclic stress–strain relationship; life assessment; meso parameters; viscoplastic constitutive model



Citation: Cao, J.; Jing, F.; Yang, J. Thermal-Mechanical Fatigue Behavior and Life Assessment of Single Crystal Nickel-Based Superalloy. *Crystals* **2023**, *13*, 780. <https://doi.org/10.3390/cryst13050780>

Academic Editor: Hongbin Bei

Received: 22 March 2023

Revised: 1 May 2023

Accepted: 2 May 2023

Published: 8 May 2023



Copyright: © 2023 by the authors. Licensee MDPI, Basel, Switzerland. This article is an open access article distributed under the terms and conditions of the Creative Commons Attribution (CC BY) license (<https://creativecommons.org/licenses/by/4.0/>).

1. Introduction

Air-cooled turbine blades in single crystal nickel-based superalloy are essential components in advanced aero engines. However, their life assessment remains a challenging issue due to thermal-mechanical fatigue, a typical failure mode caused by cyclical thermal and mechanical loads during operation [1,2]. In different regions of air-cooled blades, the phases between temperature and stress/strain vary significantly, which affects their fatigue life. For example, when an engine starts, the initial temperature rise rate on the outer surface of air-cooled blades exposed to the high-temperature gas is much higher than that on the inner surface in contact with the cooling airflow. As a result, the outer surface is subjected to compressive thermal stress, and the inner surface to tensile thermal stress. This means that there is approximately a 180° phase difference between temperature and stress/strain on the outer surface of the blade, known as an out-of-phase (OP) cycle, while there is almost no phase difference between the two on the inner surface of the blade cooling channel, known as an in-phase (IP) cycle [3].

Previous studies [4–7] on TMF tests of various single crystal nickel-based superalloys have revealed that the temperature cycling leads to significant asymmetry in the stress–strain curves, and the value and direction of the mean stress/strain accumulated are closely related to testing conditions such as phase angle and load control mode. The mechanical behavior of single crystal superalloys could significantly alter the damage

evolution, which ultimately affects the fatigue life of the materials under TMF conditions. Under the same mechanical loading, the TMF damage of a single crystal superalloy could be greater or less than the isothermal fatigue (IF) damage at the highest temperature of the cycles. Therefore, life assessment based on the IF testing may not always be the expected conservative in predicting TMF life.

However, under the same phase angle conditions, the trend of TMF life is similar to that of isothermal fatigue with changes in strain range, maximum temperature, and other factors. Therefore, to predict the TMF life under different loading conditions, several studies [8–11] have developed models using functions similar to the existing IF life models, such as strain-life models, strain/strain energy range partitionings, and Ostergren model, expressing the material constants as functions of phase angle and cyclic peak temperature. These models are relatively simple in form but have limited ranges constrained by temperature, strain, and their combinations.

The Neu-Sehitoglu damage model [12,13] assumes that the total damage of each TMF cycle is accumulated from fatigue, oxidation, and creep damage. By introducing phase factors in the oxidation damage term and the creep damage term, the competition between different damage types is characterized under different loads. This model can analyze the dominant failure factors according to the relative magnitudes of each damage term, thus achieving TMF life prediction under complex loads. However, the model requires a complex acquisition process due to numerous material constants, especially requiring special environmental tests to decouple the oxidation damage from the other two damage terms, which is still a challenge. In addition, the model has insufficient accuracy for cyclic asymmetry situations, as the fatigue damage is related only to the macroscopic mechanical strain range.

This paper focuses on investigating the influence of temperature cycling, phase angle, load control mode, and other factors on the mechanical behavior and fatigue life of single crystal nickel-based superalloy. TMF tests are conducted on thin-walled tubular specimens with mechanical strain control based on the typical service loads and structural characteristics of air-cooled turbine blades. Utilizing the viscoplastic constitutive model based on the slip system, the relationship between TMF damage and mesoscopic parameters of the slip system is established. Finally, a TMF life model based on mesoscopic parameters is established for the single crystal nickel-based superalloy, and a preliminary validation is carried out by combining existing test data.

2. Materials and Tests

2.1. Materials

Table 1 displays the nominal composition of DD6, a second-generation single crystal nickel-based superalloy material in the Chinese series that is comparable to CMSX-4 and PWA1484. The heat treatment process of DD6 is as follows: solution treatment at 1290 °C for 1 h, at 1300 °C for 2 h, and 1315 °C for 4 h, respectively, followed by a first-stage aging treatment at 1120 °C for 4 h and a second-stage aging treatment at 870 °C for 32 h. To align with the structural characteristics of air-cooled turbine blades [14], the TMF tests were carried out on tubular specimens with a wall thickness of 1 mm, as shown in Figure 1. The axial direction of the specimens represents the [001] orientation of the single crystal superalloy. The outer surface of the specimens was polished longitudinally, and the inner surface was honed to prevent any machining defects.

Table 1. Chemical composition of single crystal nickel-based superalloy DD6 (wt.%).

Ni	Al	Ta	W	Co	Re	Hf	Cr	Mo
Balanced	5.2~6.2	6.0~8.5	7.0~9.0	8.5~9.5	1.6~2.4	0.05~0.15	3.8~4.8	1.5~2.5

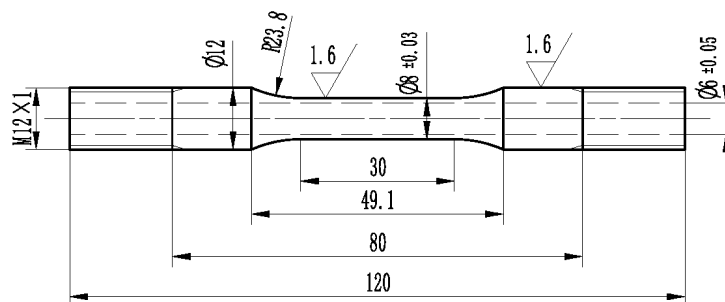


Figure 1. The schematic of thin-walled tubular specimens for the strain-controlled fatigue test (unit: mm).

2.2. Test Procedure

Previous Studies [3–7] have demonstrated a significant difference in the life trend of single crystal nickel-based materials between the strain-controlled and stress-controlled TMF tests. However, the actual loading conditions experienced by air-cooled turbine blades are somewhere between the two. In the “hot spot” or stress concentration area of the blade, the local deformation is constrained by the surrounding material, resulting in loads that are closer to those under the mechanical strain-controlled TMF test.

TMF tests were carried out using an MTS 810 servo-hydraulic test system in accordance with the ASTM E2368-10 test standard [15], including both out-of-phase and in-phase tests with a temperature range of 400~980 °C. In the out-of-phase TMF test, the phase angle between the temperature and mechanical loading is approximately 180 °C, to simulate the outer surface of the air-cooling blades when the inner cooling channels are strongly cooled. In the in-phase TMF test, however, it means that there is almost no phase difference between the temperature and mechanical loading, simulating the inner surfaces of the cooling channels. Meanwhile, the IF tests were performed with the maximum temperature of 980 °C in the TMF cycles to investigate the influence of temperature cycling.

The testing schemes of the TMF and IF tests are presented in Table 2. All the tests were tension-compression fatigue tests with a strain ratio of −1. The TMF frequency was approximately 0.01 Hz with a triangular waveform. The cyclic stress–strain data were recorded for each test so that variations in maximum and minimum strains could be examined. An electromagnetic induction heating system and a compressed air-cooling system were employed for the TMF tests. The surface temperature of the gauge section of the specimen was monitored using an S-type thermocouple combined with a thermal imager, while the axial strain was measured using a high-temperature extensometer.

Table 2. Testing matrix in strain-controlled TMF and IF test.

Type	Temperature °C	Strain Amplitude %	Strain Ratio	Cycling Time s
IP TMF	400~980	±0.55	−1	120
IP TMF	400~980	±0.50	−1	120
IP TMF	400~980	±0.45	−1	120
IP TMF	400~980	±0.40	−1	120
OP TMF	400~980	±0.55	−1	120
OP TMF	400~980	±0.50	−1	120
OP TMF	400~980	±0.45	−1	120
OP TMF	400~980	±0.40	−1	120
IF	980	±1.0	−1	8
IF	980	±0.80	−1	6.4
IF	980	±0.60	−1	4.81
IF	980	±0.50	−1	4

3. Results

3.1. Stress–Strain Relationship

The hysteresis loops of single crystal specimens under different loading conditions are shown in Figure 2, and the evolutions of the maximum stress, the minimum stress, and the mean stress with the number of cycles are shown in Figure 3. The results indicated that the mechanical stress range, hysteresis loop width and cyclic stress range increase with the increase in the strain. For the IF cycle, the hysteresis loop is approximately symmetric (Figure 2a), and the mean stress tends to evolve over most of the life zone before fracture (Figure 3a) because the elastic modulus of the material is constant as a result of the stabilization of temperature over the whole test. However, in the TMF cycle, due to the temperature dependence of the mechanical behaviors of the single crystal superalloy, the asymmetric stress–strain response is significant under the symmetric mechanical loading.

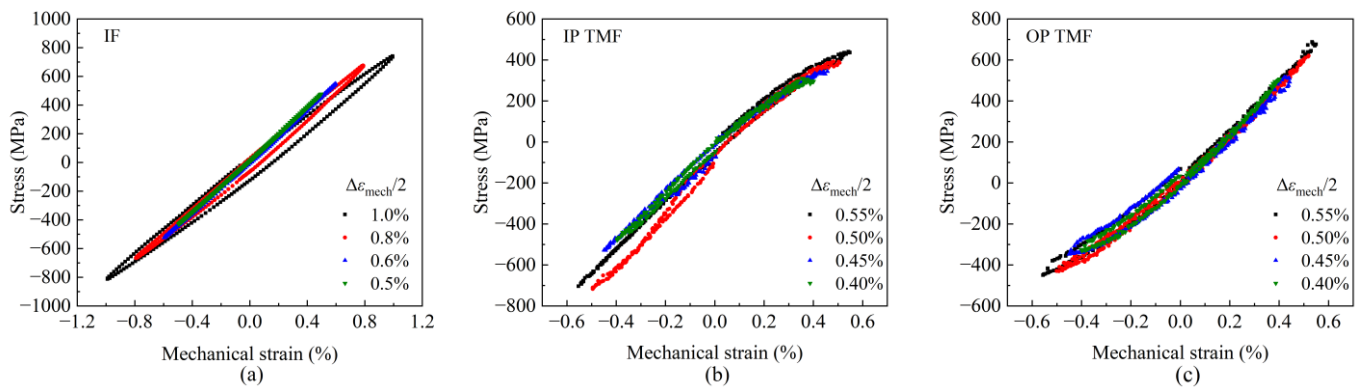


Figure 2. Hysteresis loops of the single crystal superalloy under different mechanical strain conditions: (a) IF, (b) IP TMF and (c) OP TMF.

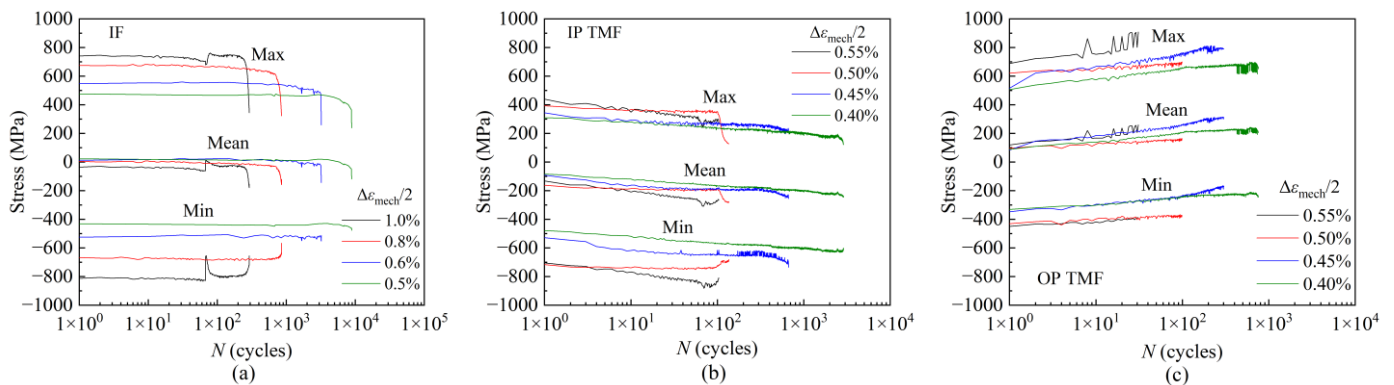


Figure 3. Cyclic maximum, minimum and mean stress versus cycle numbers for the single crystal superalloy under different mechanical strain conditions: (a) IF, (b) IP TMF and (c) OP TMF.

For the IP TMF cycle (Figure 2b), the material is subjected to tensile stress in the higher temperature stage and compressive stress in the lower temperature stage. With the increase in temperature, the ability of the single crystal superalloy DD6 to resist elasticity and inelasticity decreases, i.e., the elastic modulus decreases and the inelastic strain increases, resulting in a decrease in stress corresponding to the same mechanical strain, often called the tensile stress relaxation. This is manifested as a decrease in the stress slope of the high-temperature tensile section, and the hysteresis loop has a downward bending tendency in the tensile stress zone. These changes cause the stress peaks and valleys to shift downward, resulting in the compressive mean stress that accumulates in the compressive direction as the number of cycles increases (Figure 3b).

For the OP TMF cycle (Figure 2c), the material experiences tensile stress during the lower temperature stage and compressive stress during the higher temperature stage. Due

to the relaxation of the compressive stress generated in the high-temperature section, the hysteresis loop tends to bend upwards in the compressive stress zone. These changes cause the peak and valley stress to shift upward, resulting in a mean tensile stress that evolves towards the tensile stress as the number of cycles increases (Figure 3c). Especially, it is worth noting that in the larger mechanical strain range ($\pm 0.55\%$), the maximum tensile stress of OP TMF gradually increases with the number of cycles, which can reach the value of the plastic flow point of the material, resulting in premature structural failure. This is deemed to be the main reason why the OP TMF cycle is the most damaging [16].

It should be noted that the TMF tests presented in this study were performed by the mechanical strain control, therefore the mean strain is maintained at 0 over the cycle. However, the thermal asymmetry of the DD6 material causes the evolution of mean stress related to the phase angle. In the stress-controlled TMF test of the same material with a stress ratio of -1 , where the mean stress is kept at 0. Due to this the deformation resistance of the material decreases in the higher temperature section, the material appears softer, and its elastic modulus is lower at high-temperature loading. Therefore, for the OP TMF conditions, the hysteresis loop curves also showed upward bending in the compression loading section as the temperature increases, resulting in a mean compressive strain and accumulation in the compressive direction. For the IP TMF conditions, however, the hysteresis loops depicted a downward bending in the tensile stress zone due to a similar reason, leading to a mean tensile strain and accumulation in the tensile direction [3].

3.2. Fatigue Behavior

Figure 4 depicts the relationship between the mechanical strain amplitude and life under different test conditions. The results show that, at the same mechanical strain amplitude, the TMF life over the temperature range of $400\sim 980\text{ }^{\circ}\text{C}$ is an order of magnitude lower than the IF life at the maximum cycle temperature of $980\text{ }^{\circ}\text{C}$, indicating that the temperature cycling led to the additional material damage. Specifically, when the cyclic mechanical strain amplitude is in the range of $\pm 0.50\%$, the lifetime for IF is approximately 100 times that in the OP TMF and IP TMF. Furthermore, in the test load range, the OP TMF life is generally lower than the IP TMF life under the same load conditions. This could be due to the fact that the OP cycle generates a gradually increasing mean tensile stress, which promotes microcrack propagation and aggravates material damage to some extent, while the IP cycle generates a mean compressive stress, which inhibits crack propagation to some extent. In other words, the mechanical damage in OP TMF is greater than that in IP TMF at the same strain amplitude level and temperature range under strain-controlled conditions.

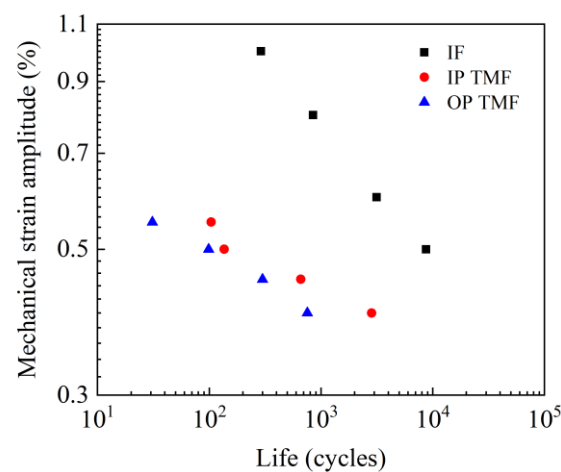


Figure 4. Mechanical strain amplitude versus life.

It is worth noting that the above life trend differs obviously from that observed in the stress-controlled test. Specifically, under strain-controlled conditions, the lifetime in TMF is consistently shorter than that in the IF, regardless of the phase angle between the

mechanical and temperature. In contrast, under stress-controlled conditions, the life of the IP TMF is the shortest, while the life of the OP TMF is the longest. The life of the IF at the highest temperature falls in between. The results suggest that whether based on the IP TMF or OP TMF or IF tests data, life assessment may not always lead to the expected conservative design in predicting TMF life.

The loading control modes have different effects on the stress–strain response of the material, which in turn affects the evolution process of the material microstructure and its damage mechanism. Therefore, it may be more feasible to build a life prediction model that is independent of the load form, rather than considering all factors that affect life.

4. Discussion

4.1. Viscoplastic Constitutive Model Based on Slip System

The Walker viscoplastic constitutive model is based on the slip system and does not involve material yielding surfaces. The model is capable of accurately describing the effects of ratcheting and stress relaxation, which has been validated on various single crystal nickel-based superalloys such as DD6 and Hastelloy-X [17,18]. DD6 is a face-centered cube (FCC) structure material with 12 octahedral slip systems and 6 cubic slip systems. In the Walker model, the parameters for the octahedral slip systems and cubic slip systems are denoted by the superscript ‘o’ and ‘c’, respectively. The stress components of the stress tensor σ can be written in the slip system coordinates using equations as follows:

$$\pi_{mn}^r = (\mathbf{m}_r^o)^T \boldsymbol{\sigma} \mathbf{n}_r^o; \pi_{mm}^r = (\mathbf{m}_r^o)^T \boldsymbol{\sigma} \mathbf{m}_r^o; \pi_{nn}^r = (\mathbf{n}_r^o)^T \boldsymbol{\sigma} \mathbf{n}_r^o; \tag{1}$$

$$\pi_{zz}^r = (\mathbf{z}_r^o)^T \boldsymbol{\sigma} \mathbf{z}_r^o; \pi_{mz}^r = \pi_{zm}^r = (\mathbf{m}_r^o)^T \boldsymbol{\sigma} \mathbf{z}_r^o; \pi_{nz}^r = \pi_{zn}^r = (\mathbf{n}_r^o)^T \boldsymbol{\sigma} \mathbf{z}_r^o; \tag{2}$$

where \mathbf{m} , and \mathbf{n} are the normal direction and the slip direction of the slip system, and \mathbf{z} is the cross-product vector of \mathbf{m} and \mathbf{n} . The unit vectors in the coordinate axes are denoted by $\mathbf{m}_r^a, \mathbf{n}_r^a$ and $\mathbf{z}_r^a = \mathbf{m}_r^a \times \mathbf{n}_r^a$, a denotes the type of slip system when $a = o$ for the octahedral slip systems and $a = c$ for the cube slip systems, r is the number of slip systems, 12 or 6. π_{mn}^r is the Schmid stress, i.e., the resolved shear stress along the slip direction in the slip plane of the stress tensor σ .

For the octahedral slip systems, the flow rule can be expressed as a power law as follows:

$$\dot{\gamma}_r^o = \left| \frac{\pi_r^o - \omega_r^o}{K_r^o} \right|^{n-1} \left(\frac{\pi_r^o - \omega_r^o}{K_r^o} \right) \tag{3}$$

where $\dot{\gamma}_r^o$ is the shear strain rate in the r -th octahedral slip system, $\pi_r^o = \pi_{mn}^o$ is the Schmid stress, n is the material constant on the sensitivity of rate, ω_r^o and K_r^o are the back stress and the drag stress, and can describe the kinematic hardening and the isotropic hardening to the deformation of the material, respectively.

The back stress and the drag stress can be written in equations as follows:

$$\dot{\omega}_r^o = \rho_1^o \dot{\gamma}_r^o - \rho_2^o \left| \dot{\gamma}_r^o \right| \omega_r^o - \rho_3^o \left| \omega_r^o \right|^{p-1} \omega_r^o \tag{4}$$

$$K_r^o = K_0^o + \rho_4^o \pi_{nz}^o + \rho_5^o \left| \Psi_r \right| \tag{5}$$

where $\rho_1^o, \rho_2^o, \rho_3^o, \rho_4^o, \rho_5^o, p$, and K_0^o are the material constants depending on the temperature, π_{nz}^o and Ψ_r are the non-Schmid stress and Takeuchi-Kuramoto stress, respectively. The Takeuchi-Kuramoto stress, Ψ_r , can be calculated according to the equations in Table 3.

Table 3. Takeuchi-Kuramoto stress in Walker viscoplastic constitutive model.

$\Psi_1 = (m_1^o)^T \sigma j$	$\Psi_2 = (m_2^o)^T \sigma k$	$\Psi_3 = (m_3^o)^T \sigma i$	$\Psi_4 = (m_4^o)^T \sigma i$
$\Psi_5 = (m_6^o)^T \sigma k$	$\Psi_6 = (m_6^o)^T \sigma j$	$\Psi_7 = (m_7^o)^T \sigma j$	$\Psi_8 = (m_8^o)^T \sigma k$
$\Psi_9 = (m_9^o)^T \sigma i$	$\Psi_{10} = (m_{10}^o)^T \sigma i$	$\Psi_{11} = (m_{11}^o)^T \sigma k$	$\Psi_{12} = (m_{12}^o)^T \sigma j$

Similarly, the flow rule, the back stress, and the drag stress in the r -th cube slip systems can be expressed as the following equations:

$$\dot{\gamma}_r^c = \left| \frac{\pi_r^c - \omega_r^c}{K_r^c} \right|^{m-1} \left(\frac{\pi_r^c - \omega_r^c}{K_r^c} \right) \tag{6}$$

$$\dot{\omega}_r^c = \rho_1^c \dot{\gamma}_r^c - \rho_2^c \left| \dot{\gamma}_r^c \right| \omega_r^c - \rho_3^c \left| \omega_r^c \right|^{q-1} \omega_r^c \tag{7}$$

$$K_r^c = K_0^c \tag{8}$$

where $\dot{\gamma}_r^c$ is the shear strain rate in the r -th cube slip system, $\pi_r^c = \pi_{mn}^c$ is the Schmid stress, $\rho_1^c, \rho_2^c, \rho_3^c, q$, and K_0^c are the material constants depending on the temperature.

The material constants in the Walker model at 780 °C and 960 °C are given in Table 4 [19]. Using the Walker viscoplastic constitutive model, the macroscopic and mesoscopic stress–strain responses of the single crystal superalloy DD6 were calculated. As shown in Figure 5, the macroscopic stress predicted by the Walker constitutive model for the DD6 specimen is well coincidental with that in the experiment.

Table 4. Material constants in Walker viscoplastic constitutive model (760 °C and 980 °C).

Octahedral Slip System			Cube Slip System		
ρ_1^o	5.0×10^6	0.5×10^6	ρ_1^c	5.0×10^6	0.5×10^6
ρ_2^o	2.083×10^4	0.25×10^4	ρ_2^c	1.852×10^4	0.442×10^4
ρ_3^o	0.0	0.0	ρ_3^c	0.0	0.0
ρ_4^o	0.15	0.0	-	-	-
ρ_5^o	0.1	-3.5	-	-	-
n	9.033	4.362	m	10.52	6.293
p	3.0	3.0	q	3.0	3.0
K_0^o	428.5	1.018×10^3	K_0^c	441.3	6.243×10^2

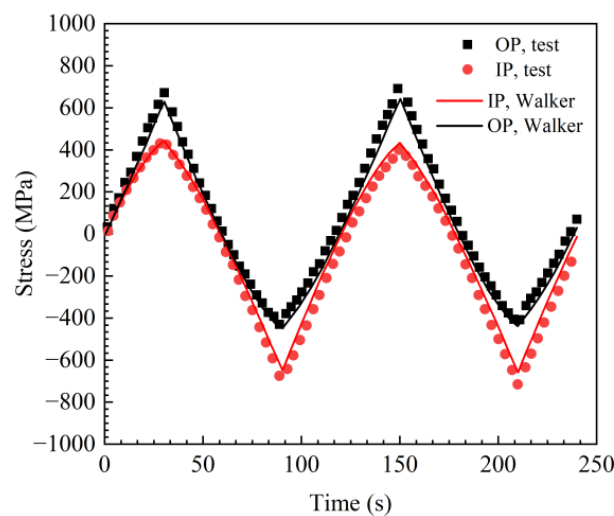


Figure 5. Calculated stress versus testing results under TMF.

4.2. Mesomechanical Parameters in TMF Testing

The evolutions of Schmid stress and slip shear strain over time for both the mechanical strain-controlled TMF (denoted by $\Delta\epsilon_{mech}$) and the stress-controlled TMF (denoted by $\Delta\sigma$) are shown in Figure 6. The stress-controlled TMF data are derived from the literature [3]. Due to the difference in cycle periods between the two load control modes, the horizontal axis in Figure 6 uses a normalized time, which is the ratio of the current time to the cycle period. This paper only presents the calculation results at the typical loads, as the evolutions of mesoscopic parameters under other conditions are similar.

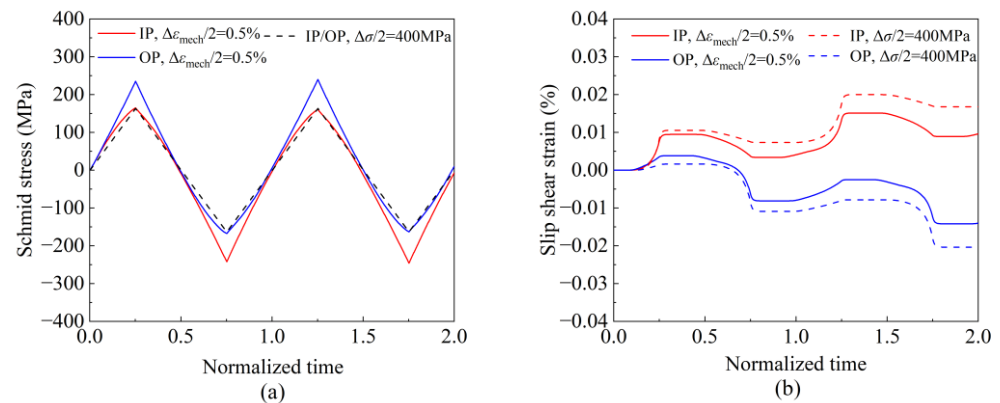


Figure 6. Mesoscopic parameters on slip systems versus time under mechanical strain-controlled and stress-controlled TMF: (a) Schmid stress versus normalized time and (b) slip shear strain versus normalized time.

The Schmid stress is obtained by decomposing the macroscopic stress tensors. In the stress-controlled TMF tests, the Schmid stress remains symmetrical both in the IP and in the OP, as shown in Figure 6a, because the macroscopic mechanical stress is symmetric under the stress ratio of -1 . In contrast, in the mechanical strain-controlled TMF tests with the strain ratio of -1 , the Schmid stress exhibits a noticeable asymmetry due to the asymmetry of the macroscopic mechanical stress induced by stress relaxation. Specifically, the mean Schmid stress of the IP cycle is negative and shifts in the compressive direction with the number of cycles, while the average value of the Schmid stress of the OP cycle was positive and shifted in the tensile direction with the number of cycles. This behavior is consistent with the evolution of measured macroscopic stress shown in Figure 3b,c. Therefore, the results depict that the Schmid stress and its related quantities could be regarded as the representative mesoscopic parameters of the material mechanical behavior.

Regardless of the control mode, the slip shear strain accumulated significantly shown in Figure 6b, indicating the irreversibility of slip. For the IP cycle, the slip shear strain remained positive, and the cycle maximum and average values of the slip shear strain gradually increased with the number of cycles. In contrast, for OP cycles, the slip shear strain is initially positive, transitions to negative values in the subsequent compression section, and accumulates in negative directions during subsequent cycles. Its trend of change reflects the influence of temperature cycles of TMF on the mechanical behavior of materials. Therefore, in the same way, the results depict that the slip shear strain and its related quantities also could be regarded as the representative mesoscopic parameters of the material mechanical behavior.

4.3. TMF Life Model Based on Mesoscopic Parameters

The mechanical response of the material and its damage evolution are dependent on the test conditions, such as the temperature-strain phase angle and the load control mode. Therefore, it is essential to select appropriate parameters for accurate TMF life modeling based on the mesoscopic stress-strain characteristics of the single crystal superalloy under different loading conditions. Previous studies [20–22] have used some parameters in the

damage rate model, including the maximum Schmid stress, the maximum slip shear strain rate, and the slip shear strain range directly related to plastic deformation. By performing calculations based on the second cycle, typical mesoscopic parameters for each slip system were determined, and then the relationship curves between the mesoscopic parameters and the TMF life were obtained, as shown in Figure 7. It is evident from Figure 7 that, in the logarithmic coordinate system, the maximum Schmid stress, the maximum slip shear strain rate, and the slip shear strain range for each test condition exhibit an approximately linear relationship with TMF life.

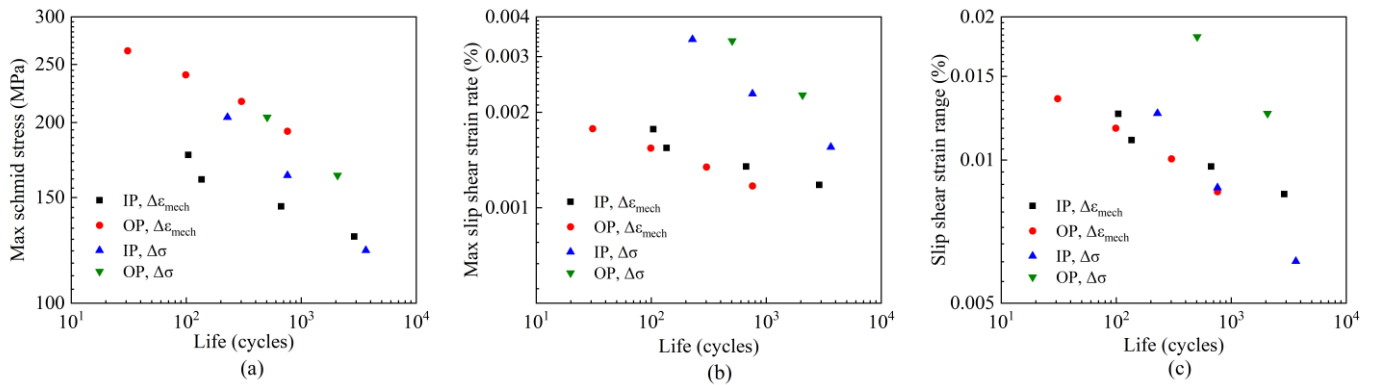


Figure 7. Microscopic parameters on slip systems versus life under TMF: (a) Max Schmid stress versus life, (b) Max slip shear strain rate versus life and (c) Slip shear strain range versus life.

Considering the difference in TMF life caused by the load control modes, based on mesoscopic parameters such as the maximum Schmid stress, maximum slip shear strain rate, slip shear strain range and Schmid stress ratio, a TMF life model in a similar form to the CDA model [22,23] is established by taking them as damage parameters based on the critical plane methods. The model is expressed as follows:

$$\log N_{\text{TMF}} = A_{\text{TMF}} + m_{\text{TMF}} \log |\pi_{\max}^{\alpha}| + n_{\text{TMF}} \log \left(\left| \dot{\gamma}^{\alpha} \right|_{\max} \right) + z_{\text{TMF}} \log |\Delta \gamma^{\alpha}| + a_{\text{TMF}} \left(\pi_{\min}^{\alpha} / \pi_{\max}^{\alpha} \right) \quad (9)$$

where N_{TMF} is the life of TMF, α denotes the type of slip system, π_{\min}^{α} and π_{\max}^{α} represent the corresponding Schmid stress values for the minimum and the maximum macroscopic stress, respectively, $\dot{\gamma}^{\alpha}$ is the slip shear strain rate and $\Delta \gamma^{\alpha}$ is the range of the slip shear strain, A_{TMF} , m_{TMF} , n_{TMF} , z_{TMF} , and a_{TMF} are the material constants, which are related to the maximum temperature of the TMF cycle and the crystal orientation and are independent of the phase angle between the temperature and the mechanical loading.

Based on the results of the strain-controlled TMF test in this paper and that of the stress-controlled TMF test previously conducted [3], combined with the calculations according to the viscoplastic constitutive model, multiple linear regression is performed on the above Equation (9), and the material constants of the model were then determined and are presented in Table 5. The results predicted by the TMF life model for different phase angles and load control modes were compared and found to fall within the twofold scatter band, as shown in Figure 8. Therefore, this model can be used to accurately evaluate the TMF life of air-cooling blades in the single crystal nickel-based material.

Table 5. Material constants in TMF life model (400~980 °C).

A_{TMF}	m_{TMF}	n_{TMF}	z_{TMF}	a_{TMF}
35.0782	−11.3985	−0.6103	3.3247	1.7894

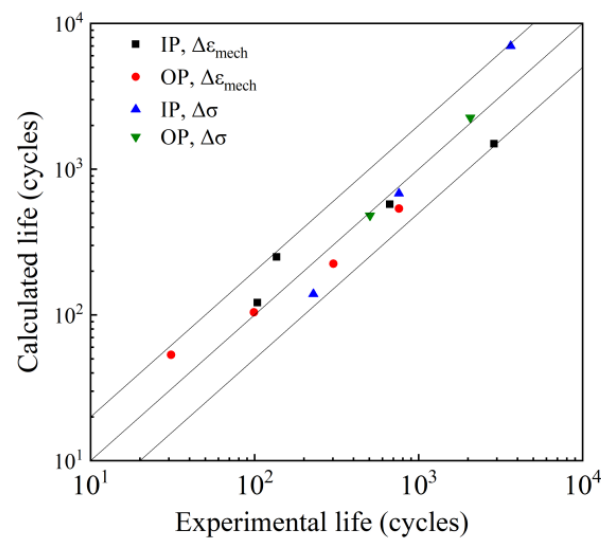


Figure 8. TMF life prediction under different phase shifts and load-controlled modes.

5. Conclusions

(1) Under strain-controlled conditions, for the same mechanical strain amplitude, the TMF life is significantly lower than the isothermal fatigue life at the maximum temperature of the TMF cycle. Moreover, the out-of-phase TMF life is generally lower than the in-phase TMF life under the same load over the range of loads investigated.

(2) Under strain-controlled conditions, temperature cycling can induce significant stress asymmetry. For out-of-phase cycles, the hysteresis loop bends upwards during the higher-temperature compression half-cycle, producing a mean tensile stress that gradually increases, which can promote micro-crack propagation and exacerbate material damage. In contrast, for in-phase cycles, the mean compressive stress generated moves gradually towards the compression direction as the number of cycles increases, thereby inhibiting crack propagation.

(3) The stress–strain response of the material can vary significantly under different load control modes, leading to different effects on the microstructure evolution and changing the damage mechanism and the life of the material.

(4) Based on the primary damage parameters identified from the stress and strain on the slip planes using the Walker viscoplasticity constitutive model, a TMF life model was developed. The model accurately predicts the TMF life for different phases and load-controlled modes within a twofold dispersion band.

Author Contributions: Conceptualization, methodology, J.C., F.J. and J.Y.; data curation, writing—original draft preparation, J.C. and F.J.; writing—review and editing, F.J. and J.Y.; project administration, J.C.; funding acquisition, J.C. and F.J. All authors have read and agreed to the published version of the manuscript.

Funding: This research was funded by the National Natural Science Foundation of China (Grant No. 51375031), and the National Science and Technology Major Project, grant number J2019-IV-0003-0070 and J2019-V-0006-0099.

Data Availability Statement: Not applicable.

Acknowledgments: The authors gratefully acknowledge the financial support from the funding.

Conflicts of Interest: The authors declare no conflict of interest.

References

1. Weijun, Z. Thermal mechanical fatigue of single crystal superalloys: Achievements and challenges. *Mater. Sci. Eng. A* **2016**, *650*, 389–395.
2. Jones, J.; Whittaker, M.; Lancaster, R.; Williams, S. The influence of phase angle, strain range and peak cycle temperature on the TMF crack initiation behaviour and damage mechanisms of the nickel based superalloy, RR1000. *Int. J. Fatigue* **2017**, *98*, 279–285. [[CrossRef](#)]
3. Fulei, J.; Kanghe, J.; Bin, Z.; Dianyin, H.; Rongqiao, W. Experimental research on thermomechanical fatigue in nickel based single crystal superalloy DD6. *J. Aerosp. Power* **2018**, *33*, 2965–2971.
4. Amaro, R.; Antolovich, S.; Neu, R.; Staroselsky, A. On thermo-mechanical fatigue in single crystal Ni-base superalloys. *Procedia Eng.* **2010**, *2*, 815–824. [[CrossRef](#)]
5. Hynunuk, H.; Jeong-gu, K.; Baiggyu, C.; Insoo, K.; Youngsoo, Y.; Changyong, Y. A comparative study on thermomechanical and low cycle fatigue failures of a single crystal nickel-based superalloy. *Int. J. Fatigue* **2011**, *33*, 1592–1599.
6. Jinjiang, Y.; Guoming, H.; Zhaokuang, C.; Xiaofeng, S.; Tao, J.; Zhuangqi, H. High temperature thermo-mechanical and low cycle fatigue behaviors of DD32 single crystal superalloy. *Mater. Sci. Eng. A* **2014**, *592*, 164–172.
7. Junjie, Y.; Fulei, J.; Zhengmao, Y.; Kanghe, J.; Dianyin, H.; Bin, Z. Thermomechanical fatigue damage mechanism and life assessment of a single crystal Ni-based superalloy. *J. Alloys Compd.* **2021**, *872*, 159578.
8. Cunha, F.; Dahmer, M.; Chyu, M. Thermal-mechanical life prediction system for anisotropic turbine components. *J. Turbomach.* **2006**, *128*, 240–250. [[CrossRef](#)]
9. Gomez, T.; Awarke, A.; Pischinger, S. A new low cycle fatigue criterion for isothermal and out-of-phase thermomechanical loading. *Int. J. Fatigue* **2010**, *32*, 769–779. [[CrossRef](#)]
10. Amaro, R.; Antolovich, S.; Neu, R.; Fernandez-Zelaia, P. Thermomechanical fatigue and bithermal–thermomechanical fatigue of a nickel-base single crystal superalloy. *Int. J. Fatigue* **2012**, *42*, 165–171. [[CrossRef](#)]
11. Vacchieri, E.; Holdsworth, S.; Poggio, E.; Villari, P. Service-like TMF tests for the validation and assessment of a creep-fatigue life procedure developed for GT blades and vanes. *Int. J. Fatigue* **2017**, *99*, 216–224. [[CrossRef](#)]
12. Vose, F.; Becker, M.; Fischersworing, B.; Hackenberg, H. An approach to life prediction for a nickel-base superalloy under isothermal and thermo-mechanical loading conditions. *Int. J. Fatigue* **2013**, *53*, 49–57. [[CrossRef](#)]
13. Abdullahi, A.; Samir, E.; Panagiotis, L.; Riti, S. Aero-engine turbine blade life assessment using the Neu/Sehitoglu damage model. *Int. J. Fatigue* **2014**, *61*, 160–169.
14. Rongqiao, W.; Kanghe, J.; Fulei, J.; Dianyin, H. Thermomechanical fatigue failure investigation on a single crystal nickel superalloy turbine blade. *Eng. Fail. Anal.* **2016**, *66*, 284–295.
15. ASTM E2368-10; Standard Practice for Strain Controlled Thermomechanical Fatigue Testing. ASTM: West Conshohocken, PA, USA, 2010; pp. 1–10.
16. Kersey, R.; Staroselsky, A.; Dudzinski, D.; Genest, M. Thermomechanical fatigue crack growth from laser drilled holes in single crystal material. *Int. J. Fatigue* **2013**, *55*, 183–193. [[CrossRef](#)]
17. Rongqiao, W.; Fulei, J.; Dianyin, H. Fatigue life prediction model based on critical plane of nickel-based single crystal superalloy. *J. Aerosp. Power* **2013**, *28*, 2587–2592.
18. Jordan, E.; Shixiang, S.; Walker, K. The viscoplastic behavior of Hastelloy-X single crystal. *Int. J. Plast.* **1993**, *9*, 119–139. [[CrossRef](#)]
19. Fulei, J.; Shibai, T.; Junjie, Y. Influence of small hole on thermal mechanical fatigue in single crystal superalloy. *J. Aerosp. Power* **2021**, *36*, 1669–1679.
20. Tinga, T.; Brekelmans, W.; Geers, M. Time-incremental creep-fatigue damage rule for single crystal Ni-base superalloys. *Mater. Sci. Eng. A* **2009**, *508*, 200–208. [[CrossRef](#)]
21. Rongqiao, W.; Bin, Z.; Dianyin, H.; Kanghe, J.; Jianxin, M.; Fulei, J. A critical-plane-based thermomechanical fatigue lifetime prediction model and its application in nickel-based single-crystal turbine blades. *Mater. High Temp.* **2019**, *36*, 325–334.
22. Fulei, J.; Rongqiao, W.; Dianyin, H.; Kanghe, J. Damage parameter determination and life modeling for high temperature fatigue of nickel-based single crystal superalloys. *Acta Aeronaut. Astronaut. Sin.* **2016**, *37*, 2749–2756.
23. Rongqiao, W.; Kanghe, J.; Dianyin, H.; Fulei, J.; Xiuli, S. High temperature fatigue life model for single crystal nickel superalloy based on principal component analysis. *J. Aerosp. Power* **2016**, *31*, 1359–1367.

Disclaimer/Publisher’s Note: The statements, opinions and data contained in all publications are solely those of the individual author(s) and contributor(s) and not of MDPI and/or the editor(s). MDPI and/or the editor(s) disclaim responsibility for any injury to people or property resulting from any ideas, methods, instructions or products referred to in the content.